Ultrathin films of three-dimensional topological insulators by vapor-phase epitaxy: Surface dominant transport in a wide temperature range as revealed by measurements of the Seebeck effect

Stephane Yu Matsushita, Kim-Khuong Huynh, and Katsumi Tanigaki

Phys. Rev. B **99**, 195302 — Published 13 May 2019

DOI: 10.1103/PhysRevB.99.195302

Ultrathin film of 3D topological insulators by vapor-phase epitaxy: Surface dominant transport in wide temperature revealed by Seebeck measurement

Stephane Yu Matsushita,[1*] Kim-Khuong Huynh,[2] and Katsumi Tanigaki[1,2 **]

[1]*Department of Physics, Graduate School of science, Tohoku University, Sendai 980-8578, Japan*

[2]*WPI-Advanced Institute for Materials Research, 2-1-1 Katahira, Aoba-ku, Sendai, Miyagi, 980-8578, Japan*

*E-mail address: *m.stephane@m.tohoku.ac.jp, **tanigaki@m.tohoku.ac.jp

PACS numbers: 73.25.+i, 73.50.Lw, 72.20.My

Abstract

Realization of intrinsic surface dominant transport in a wide temperature region for a topological insulators (TIs) is an important frontier research in order to promote the progresses of TIs towards the future electronics. We report here systematic measurements of longitudinal electrical transport, Shubnikov-de-Haas (SdH) quantum oscillations, Hall coefficient ($R_{\mathrm{H}}^{2\mathrm{D}}$), and Seebeck coefficient as a function of film thickness (d) and temperature using high quality $Bi_{2-x}Sb_xTe_{3-y}Se_y$ (BSTS) single crystal thin films grown by physical vapor-phase deposition. The thickness dependence of sheet conductance and Seebeck coefficient clearly show the suppression of semiconducting hole carriers of bulk states by reducing film thickness, reaching to the surface dominant transport at below d_c=14 nm. Quantitative arguments are made as to how the contribution of itinerant carrier number (n) can be suppressed, using both $R_{\mathrm{H}}^{2\mathrm{D}}$ ($n_{\mathrm{Hall}}^{2\mathrm{D}}$) and SdH ($n_{\mathrm{SdH}}$). Intriguingly, the value of $n_{\mathrm{Hall}}^{2\mathrm{D}}$ approaches to be twice of n_{SdH} below d_c. While $R_{\mathrm{H}}^{2\mathrm{D}}$ shows a negative sign in whole temperature region, a change from negative to positive polarity is clearly observed for S at high temperatures when d is thick. We point out that this inconsistency observed between $R_{\mathrm{H}}^{2\mathrm{D}}$ and S is intrinsic in 3D-TIs and its origin is the large difference in carrier mobility between the bulk and the topological surface. We propose that Seebeck coefficient can become a convenient and effective tool to evaluate the intrinsic topological surface transport of 3D-TIs in the absence of magnetic field.

1. Introduction

Topological insulators (TIs) have currently been attracting much attention from the viewpoint of contemporary materials science generating new electronic states, such as gapless helical massless Dirac fermions on two-dimensional (2D) surface or one-dimensional (1D) edge [1-3]. The existence of such special energetic states on the topological surface states has unambiguously been confirmed by surface sensitive measurements of angle and spin resolved photoemission spectroscopy [4-7]. Although many theoretical approaches suggest exotic physical properties as well as novel applications of TIs, clear clarification of such physical properties has still been difficult experimentally because itinerant carriers thermally generated from the bulk bands are frequently involved in experimental observations of physical properties. Therefore, one of the most important requirements in order to unveil the intrinsic physical properties of TIs is how we can evaluate the physical properties by minimizing and discriminating the contribution of bulk carriers when we measure the properties of topological surface Dirac states (TSDS). This can be realized in principle by either tuning the Fermi level (E_F) inside the bulk gap or growing high quality ultra-thin films to reduce the bulk contribution in total. The E_F is known to be engineered in synthesis by the concept of "charge-defect-controlling", and two kinds of highly bulk insulating 3D-TIs of $Bi_{2-x}Sb_xTe_{3-y}Se_y$ (BSTS) and Sn-$Bi_{1.1}Sb_{0.9}Te_2S$ (Sn-BSTS) are presently proposed [8-14]. As for the reduction in film thickness, on the other hand, the suppression of the bulk in thin films can be recognized only at low temperatures, but no systematic study has been carried out and common experimental consensus has not been achieved to confirm firmly whether the surface dominant transport can be realized in a wide range of temperature.

In general, Hall measurement is a common and useful technique to evaluate contributions of conduction channels in electrical transport. In principle, whether electrical conduction of a material is made via either of single or multi carriers can be evaluating by the transverse electrical transport R_{yx} (B) (Hall effect: R_H); a linear progression as a function of B is essential for single-channeled carriers, while a non-linear one is observed for multi-channeled carriers. The non-linear term of R_{yx} (B) of 3D-TIs, caused by the large mobility difference between the surface and bulk carriers that is robustly protected by topology, can only be evident under high B above 10 T. It is, however, not generally easy for interpreting such experimental data to deduce a firm conclusion as to whether predominant properties resulting from TSDS are observed from the linear dependence of R_{yx} (B) and therefore debate still continues. The surface dominant electrical transport can qualitatively be discussed from the temperature (T) dependence of longitudinal and transverse electrical transport or the thickness (d) dependence of sheet resistance ($R_\square$). In principle, more accurate analytical discussion can be possible by employing both non-linearity in R_H and Shubnikov-de-Haas (SdH) quantum oscillations under extremely high B field [15]. However, valid combined-measurements of R_H and SdH are required to be carried out at low T below 10 K under high B, and therefore do not allow one to make direct discussions at room temperature.

Another method to distinguish the carrier type is to measure the Seebeck coefficient (*S*) [16]. The polarity of *S* reflects the polarity of the dominant carrier as well as R_H, i.e. positive for p-type carrier and negative for n-type carrier. Moreover, it is able to distinguish whether the carrier is semiconducting or metallic by measuring the *T* dependence of *S,* because *S* shows non-linear *T* dependence for semiconducting carriers whereas linear *T* dependence can be observed in the metallic regime. Recently, we reported the thickness dependence of Seebeck coefficient and revealed the surface dominant *S* for BSTS thin film crystals, which can clearly be judged from both the different polarity as well as the *T* dependence between the p-type semiconducting bulk carriers and the n-type carriers of TSDS [17]. Measurements of *S* in 3D-TI thin films have also been carried out for $Bi_{2-x}Sb_xTe_3$ (BST) alloys. J. Zhang *et al*., tuned E_F by chemical doping on BST thin films and observed inconsistent polarity between the Hall and the Seebeck coefficient [18]. Although this is considered to be caused by the large difference in mobility between the topological surface and the bulk carriers in 3D-TI, the discussion remains still ambiguous due to the coexisting electronic states of bulk and surface. Considering the situation described so far, accurate discussions on the separate contributions are indeed important as a function of thickness (*d*) and temperature (*T*), which can be viewed simultaneously from the two complementary experimental observation of Hall and Seebeck coefficients.

Here, we report our systematic experimental observations of a set of important electrical transport data of sheet resistance ($R_{\square}$), SdH quantum oscillations, Hall coefficient (R_H^{2D}), and Seebeck coefficient (*S*) as a function of both *d* and *T* using high quality BSTS single crystal thin films. In order to make unambiguously quantitative discussions on the contribution and the differentiation between the topological surface and the bulk state, we grow 3D-TI BSTS thin films with thickness ranging from 5 to 75 nm grown by employing non-catalytic vapor phase crystal growth reported elsewhere [14,19]. $R_{\square}$ and *S* of BSTS films employed in the present experiments show an accurate systematic shift from the bulk/surface coexisting regime to the surface dominant one with a reduction in *d*. The *S* values for thinner films clearly show a linear *T*-dependence with negative polarity from 300 K to 2K, indicating a surface dominant transport of metallic n-type surface carriers in a wide-*T* region. The suppression in contribution of bulk carriers in thin films is quantitatively discussed based on the carrier densities of n_{Hall}^{2D} and n_{SdH} to be evaluated by R_H^{2D} and SdH measurements, respectively. The discrepancy between n_{Hall}^{2D} and n_{SdH} experimentally determined by the two methods becomes smaller and importantly approaches to be constant as *d* of 3D-TI decreases. The value of n_{SdH} approaches to a half value of n_{Hall}^{2D} as *d* is decreases. We propose that *S* can be a very sensitive and convenient probe even in the absence of *B* and at high *T*, and can be employed for accurate evaluation of TIs in order to judge whether the surface dominant electronical transport can be realized.

2. Experimental

BSTS single crystal thin films with 1 cm^2 large in size were grown on mica substrate with a catalyst-free epitaxial physical vapor deposition (PVD) method using a dual-quartz tube system, the details of which were reported elsewhere [14,19]. First, a highly insulating $Bi_{1.5}Sb_{0.5}Te_{1.7}Se_{1.3}$ single crystal was synthesized as a source material. The purity of the elements employed for single crystal growth was Bi (5N), Sb (5N), Te (5N), and Se (5N). The source material was then placed into a dual-quartz tube system, and the system was evacuated at 10^{-1} Pa with a vacuum pump. A mica substrate was located at the other end of the dual quartz tube to grow BSTS single crystal thin films with various thicknesses. The quality of the grown films was characterized by energy dispersive X-ray (EDX) spectroscopy, Raman spectroscopy and X-Ray diffraction (XRD). The thickness of the film was measured by atomic-force-microscopy (AFM) (See Fig. S1 in Supplemental Material [20]).

Resistivity and Hall measurements were carried out by a common five probe method using the Physical Properties Measurement System (PPMS, Quantum Design). A magnetic field of 0 to ±9 T perpendicular to the film surface was applied for Hall and magnetoresistance measurements. For the measurement of Seebeck coefficient, a home-built device was used as described elsewhere [17].

3. Results

3.1 Electrical resistivity.

Figure 1(a) shows T evolution of the 2D sheet resistances ($R_{\square}$) of five BSTS thin films with different thicknesses (75 nm, 36 nm, 14 nm, 7 nm, and 5 nm). The observed values of $R_{\square}$ at 300 K are $R_{\square}$=1.6 (75 nm), 4.3 (36 nm), 14.5 (14 nm), 12.9 (7 nm) and 14.8 kΩ (5 nm). These high $R_{\square}$ values can ensure that good bulk insulation is realized in our BSTS thin films. It is important to see that $R_{\square}$ at 300 K shows a large increase in value with a decrement in film thickness from 75 nm to 14 nm, while no significant difference was observed below 14 nm. For the thick film of 75 nm, a typical T dependence similar to that of insulating bulk specimen was observed, where $R_{\square}$ reached the maximum at around 105 K and started to decrease as T became further low. The insulating property gradually smeared out for the 36 nm film, and became less with a further reduction in d, leading to an intrinsic metallic T dependence of the nontrivial metallic TSDS emerging over an entire T range.

Figure 1(b) shows the thickness dependence of sheet conductance ($G_{\square}$) of BSTS films at 300 K and 2 K. In both temperatures, $G_{\square}$ shows a markedly different behavior between above and below the critical thickness of d_c=14 nm; a linear increase with an increase in d was obseved above d_c, while it became nearly constant below d_c. The linear d dependent term in the equation is attributed to the contribution of the bulk carriers and the constant term can be ascribed to that of the TSDS. Employing a two-layer parallel

connection circuit model as $G_{\square} = G_{\square}^{s} + \sigma_b d$, where $G_{\square}^{s}$ and σ_b are the sheet conductance of the TSDS and the bulk conductivity, respectively, σ_b was estimated to be 52.4S cm^{-1} at 2 K and 92.5 S cm^{-1} at 300 K. The decrease in σ_b value as a function of T can be ascribed to the *T*-dependent thermally activated carriers generated in the bulk. On the other hand, $G_{\square}^{s}$ below 14 nm increases monotonically from 0.71 at 300 K to 1.02 × 10^{-4} S at 2 K, where the latter value at 2 K is comparable with those reported previously [10,14,15]. A nearly identical constant sheet conductance was observed in the entire temperature range of 300 K to 2 K, being indicative of an experimental fact that a topological layer with two-dimensional Dirac carriers exists with ineligible dependence on *d* from the viewpoint of electrical transport.

3.2 Seebeck coefficient

Figure 2 shows *T* dependence of Seebeck coefficient (*S*) for five BSTS thin films. The 75 nm-BSTS showed a p-type *S* with a nonlinear *T* dependence with positive charge polarity and a maximum value of S=193 μVK^{-1} at 300 K, which showed its sign change to a negative one at 100 K and a *T*-linear dependence by approaching to 2 K. The nonlinear *T* dependence of *S* at high *T*'s can frequently be observed in semiconductors when hole carriers are generated in a valence band via thermal excitations of electrons to an upper impurity trapping level. On the other hand, the linear *T* dependence is a typical behavior for metals [21,22]. The experimental result of 75 nm-BSTS indicates that the dominant carriers evidently change from semiconducting holes of the bulk to metallic electrons of the TSDS by decreasing *T*. This is consistent with the observations of $R_{\square}$ as described earlier. By reducing *d* to 36 nm, the value of *S* became 44 μVK^{-1} and its sign changed to be negative even at a higher *T* of 193 K. On further reduction in *d*, the 14, 7, and 5 nm-BSTSs showed a negative *S* in the entire *T* region with a similar linear *T* dependence, importantly indicating a fact that electrons are dominant in metallic TSDS [17]. The value of *S* became almost independent of *d* below ca. 50 K. These results are consistent with the ideal situation that thermoelectric transport of TSDS is independent of the film thickness, whereas the contribution of the bulk varies with decreasing *d*. It is noted again that the values of *S* for the BSTS films below 14 nm were almost independent of *d* in the entire *T*, which is consistent with the results of $R_{\square}$ in Fig. 1b as described earlier. As being described in this paragraph, the surface dominant transport in a wide *T* range from 300 K to 2 K can be realized around at *d*=14 nm.

3.3 Hall coefficient

In order to quantitatively confirm the surface dominant transport, we carried out simultaneous measurements of Hall resistivity and SdH oscillations. Figure 3(a) and (b) show the magnetic field (*B*)

dependences of transverse sheet resistance (R_{yx}) of BSTS films at 300 K and 2 K, respectively. Considering the results of *S* described earlier, R_{yx} should be non-linear for thick films due to the two types of carriers of bulk and TSDS. However, in both temperatures, R_{yx} shows a negative slope for all film thicknesses with almost a linear *B* dependence. This can be understood by both small carrier concentration and low mobility of the bulk in BSTS, which shift the non-linear term of R_{yx} to be observed in a high *B* fields above 10 T. Therefore, we were able to estimate the two-dimensional hall coefficient ($R_{\mathrm{H}}^{2\mathrm{D}}$) from a linear fitting under low *B* from -1 T to 1 T, where the high mobility carriers of the TSDS are dominant. Figure 3(c) shows $R_{\mathrm{H}}^{2\mathrm{D}}$ at various *T*'s. The sign of $R_{\mathrm{H}}^{2\mathrm{D}}$ was always negative, indicating that the dominant transport carriers are electrons of on the TSDS.

The 2D-carrier density ($n_{\mathrm{Hall}}^{2\mathrm{D}}$) was estimated from $R_{\mathrm{H}}^{2\mathrm{D}}$ as shown in Fig. 3(d). For the 75 nm-BSTS, $n_{\mathrm{Hall}}^{2\mathrm{D}}$ shows a strong *T* dependence, where $n_{\mathrm{Hall}}^{2\mathrm{D}}$ decreases exponentially from 2.5×10^{14} cm^{-2} at 300 K to 3.1×10^{13} cm^{-2} at 2 K. The *T* dependence of $n_{\mathrm{Hall}}^{2\mathrm{D}}$ became much weaker by reducing the film thickness and reached a nearly constant value of 6.3×10^{12} cm^{-2} at 5 nm. The strong *T* dependence of $n_{\mathrm{Hall}}^{2\mathrm{D}}$ is due to the contribution of the bulk carriers, and therefore the intrinsic Hall coefficient ($R_{\mathrm{H}}^{2\mathrm{D}}$) of the surface channels becomes underestimated and consequently gives overestimated $n_{\mathrm{Hall}}^{2\mathrm{D}}$ at high *T*s. Nearly *T*-independent $n_{\mathrm{Hall}}^{2\mathrm{D}}$ for both 5 and 7 nm-BSTSs indicates that the contribution of bulk carriers to the electrical transport can negligibly be small in these thicknesses. The conclusion described here is consistent with those deduced from $R_{\square}$ and *S* measurements as described earlier.

3.4 Quantum oscillation

SdH quantum oscillations of 75 nm and 5 nm-BSTS observed at 2 K are shown in Fig. 4. Figure 4(a) and (c) were the ΔR-1/*B* plots obtained with correction of the background in polynomial fitting, where clear SdH oscillations can be seen as a function of 1/*B*. These quantum oscillations were observed for all BSTS films. By carrying out fast Fourier transformation (FFT) of ΔR-1/*B*, two specific components of B_{F} =32.4 and 56.8 were revealed for the 75 nm-BSTS, whereas one component of B_{F} =123.9 was achieved for the 5 nm-BSTS as shown in Fig. 4(b) and (d).

For more clear understanding, Fan-diagram plots were made for 75 and 5 nm-BSTSs as shown in Fig.4 (e). The experimental line in black indicates the peak and valley positions for the 75 nm BSTS, and the red one is for the 5 nm-BSTS. Both black and red lines were drawn from the linear fitting of the plot using the value of 1/B_{F} evaluated from the FFT analyses. Two conducting channals for the 75 nm film showed different berry phases of $\beta = 0.00$ (B_{F} =56.8) and 0.55 (B_{F} =32.4), and the value of conducting channel of 5 nm film was $\beta = 0.64$ (B_{F} =123.9). Importantly, carriers of both non-trivial TSDS (β=1/2)

and trivial bulk state (β=0) were observed in the case of the thick 75 nm-BSTS, while only TSDS state was observed in the thin 5 nm-BSTS. The disappearance of the bulk states for the thin 5 nm-BSTS can be reasonable considering the larger reduction of the bulk contribution as *d* reduces.

In the case of ultra-thin film around a few nm in thickness, the top and bottom TSDSs could be hybridized and an energy gap is opened on the TSDS band. Such a surface gap was observed in Bi_2Se_3 in the film thickness below 5 QL (5 nm) by ARPES and transport measurements [23,24]. In our previous work on the thermoelectric properties of BSTS films [17], we also reported a similar surface gap in the 4-QL (4 nm) film. Compared to these previous works, the 5 nm-BSTS in the present work seems to be located at the threshold of thickness for opening a hybridization energy gap. In the gapped states, the TSDSs lose their topological properties of the berry phase and the weak anti-localizations (WAL). In the present case, however, the top and the bottom surfaces of 5 nm-film are considered to be not hybridized, because a typical berry phase with β=0.64 (Fig.3 (e)) in the Fan diagram and the WAL behavior in the magnetoresistance curve were observed (See Fig. S2 in Supplemental Material [20]). Since 5 nm is close to the border of the hybridization, it may be possible that a small gap that does not change the electrical transport properties of TSDS exists within a few meV [24].

4. Discussion

4.1 Comparison of carrier density between Hall and SdH measurements

Based on the experimental data and their analyses of SdH quantum oscillations described earlier, the 2D-carrier densities of TSDS were estimated as $n_{\mathrm{SdH}} = 7.8 \times 10^{11}$ cm^{-2} for the 75 nm-BSTS and 3.0×10^{12} cm^{-2} for the 5 nm-BSTS. It is noted that the carrier density of the 75 nm-BSTS deduced from SdH is smaller by two orders in magnitude than that evaluated from Hall measurements ($n_{\mathrm{Hall}}^{\mathrm{2D}} = 3.1 \times 10^{13}$ cm^{-2}), while the two values were within the same order in the case of the 5 nm-BSTS ($n_{\mathrm{Hall}}^{\mathrm{2D}} = 5.73 \times 10^{12}$ cm^{-2}). These experimental observations provide us the following information. Generally, when a material has two types of conducting channels for n- and p-carriers, linear fitting of the R_{yx} will underestimate the Hall coefficient (an overestimate of $n_{\mathrm{Hall}}^{\mathrm{2D}}$) due to the compensation in sign between electrons and holes. On the other hand, SdH oscillations can extract the intrinsic carrier density for individual channels separately by deconvoluting the experimental data.

Figure 5 shows the thickness dependence of estimated 2D-carrier densities of TSDS evaluated from Hall measurements ($n_{\mathrm{Hall}}^{\mathrm{2D}}$) and SdH measurements ($n_{\mathrm{SdH}}$) at 2 K. It is clear that the discrepancy between these two values becomes smaller as the film thickness is reduced. Importantly, the ratio of the two carrier densities $n_{\mathrm{Hall}}^{\mathrm{2D}}/n_{\mathrm{SdH}}$ becomes constant below the film thickness of 7 nm, as shown in the inset of Fig. 5. Since two conducting surface channels exist on the top and the bottom surfaces of TSDS in 3D-TIs and the carrier density deduced from the Hall measurements is the sum of these two surfaces, the value of

$n_{\mathrm{Hall}}^{2\mathrm{D}}$ should be the twice of n_{SdH}. Consequently, our experimental results indicate that the contribution of the bulk carriers becomes negligible for films below 7 nm in thickness so that the intrinsic nontrivial pure TSDS can be observed.

In order to verify the above discussion, we fitted the Hall resistivity of thin films by employing a two-carrier type model (See supplementary Material [20]). As shown in Fig. S3, the R_{yx} of 7 nm-film can be fitted in a reasonable fashion by the two n-type carriers ($n_1 = 1.9 \times 10^{12}$ cm^{-2}, $\mu_1 = 1078$ cm^{2}V^{-1}s^{-1}, $n_2 = 1.8 \times 10^{12}$ cm^{-2}, $\mu_2 = 1076$ cm^{2}V^{-1}s^{-1}), supporting the electrical transport consisting of the two surface states. For the 5 nm-film, on the other hand, we evaluated also a contribution of p-type carrier ($n_1 = 1.5 \times 10^{11}$ cm^{-2}, $\mu_1 = 2280$ cm^{2}V^{-1}s^{-1}) in addition to n-type carrier ($n_1 = 3.0 \times 10^{12}$ cm^{-2}, $\mu_1 = 850$ cm^{2}V^{-1}s^{-1}). As we discussion in section 3.3, the two surface states may start to hybridize at 5 nm in thickness and the band configuration start to be modified between the top and the bottom surfaces.

4.2 The inconsistency of Seebeck and Hall coefficients

It is importantly noted that the sign of $R_{\mathrm{H}}^{2\mathrm{D}}$ was always negative even in the thick films of 75 and 36 nm-BSTS, which contradicts to the results obtained from the *S* measurements, where a positive *S* value was observed for the thick films as described earlier. In general, the polarity of Seebeck and Hall coefficients should be consistent with each other. The different contribution observed in the present studies between Hall and Seebeck can be interpreted in terms of the large difference in carrier mobility between the trivial bulk and the non-trivial surface states of TIs as explained as follows:

Applying a two-parallel circuit model of a bulk and a surface, Seebeck and Hall coefficients can be described as

$$S = \frac{\sigma_b t S_b - G_{\square}^{s} S_s}{\sigma_b t + G_{\square}^{s}} = -\frac{G_{\square}^{s} S_s}{G_{\square}}\left(1 - \frac{\sigma_b t}{G_{\square}^{s}}\frac{S_b}{S_s}\right) \qquad (1)$$

$$R_{\mathrm{H}}^{2\mathrm{D}} = \frac{\sigma_b t \mu_b - G_{\square}^{s} \mu_s}{\left(\sigma_b t + G_{\square}^{s}\right)^2} = -\frac{G_{\square}^{s} \mu_s}{G_{\square}^{\ 2}}\left(1 - \frac{\sigma_b t}{G_{\square}^{s}}\frac{\mu_b}{\mu_s}\right) \qquad (2)$$

, where σ_b, μ_b, S_b are the electrical conductivity, the mobility, and the Seebeck coefficient of bulk, $G_{\square}^{s}$, μ_s, S_s are the sheet conductance, the mobility, and the Seebeck coefficient of surface, and *t* is the thickness of films. By comparing these two equations, it is clear that the difference in sign between the two coefficients arises from the ratio of $\frac{S_b}{S_s}$ and $\frac{\mu_b}{\mu_s}$. According to the linear fitting analyses of sheet conductance in Fig. 1(b) as described earlier, the ratio of $\frac{\sigma_b t}{G_{\square}^{s}}$ is 10 and 5 for 75- and 36 nm-BSTS at 300 K, respectively. Using the *S* value of 193 μVK^{-1} for the 75 nm-BSTS as S_b, and -45 μVK^{-1}for the 5 nm-BSTS as S_s, the

product becomes $\frac{\sigma_b t}{G_{\square}^{S}} \frac{S_b}{S_s} = 43$ and 21 for the 75 nm and the 36 nm-BSTS, respectively. When this multiplied value is larger than 1, a positive *S* can be observed.

On the other hand, Dirac electrons of surface have a large mobility due to the topologically prohibited backward scattering, resulting in a greatly smaller value of $\frac{\mu_b}{\mu_s}$. The mobility of TSDS can be estimated from the SdH oscillations using the following equation:

$$\Delta R_{xx} = A \exp(-\pi/\mu^* B) \cos[2\pi(B_F/B + 1/2 + \beta)] \quad (3)$$

where A is the amplitude, μ^* is the carrier mobility, B_F is the periodic frequency of the oscillations, and β is the Berry phase [10,25,26]. Fitting was carried out by employing the evaluated B_F and β value from FFT and fan-diagram plot analyses (B_F = 77.5 and β = 0.35) for the 7 nm-BSTS as a typical example as shown in Fig. 6. The value of μ^* for TSDS in the Dirac electron pocket was evaluated to be 1078 $cm^2 V^{-1} s^{-1}$, which is similar to those in the previous measurements [14]. A typical value of the bulk mobility of BSTS is only several tens $cm^2 V^{-1} s^{-1}$ [15, 27-29] to give $\frac{\mu_b}{\mu_s} \sim 0.01$, and a negative value of R_H^{2D} can be observed. The negative polarity of R_H^{2D} in 300 K in the present experiments indicates that the mobility of the surface electron carriers is still quite larger than that of the bulk holes even in the high *T* region.

Generally, a two-channel model is discussed for thermoelectric and magnetoelectric transports by using electronic conductivity (σ_b/σ_s). That is also the case in the previous work in BST thin films reported by J. Zhang et al. [18]. In addition to this general concept, we pointed out here that the film thickness is also an essential parameter to determine the transport properties of 3D-TIs. As can be known from equation (1) and (2), the electronic transport of 3D-TIs should be discussed by not only conductivity (σ_b/σ_s) but also sheet conductance ($\sigma_b t/G_{\square}^{S}$), because the dimension of the two conduction channels is different from each other. Our quantitative discussions described earlier indicate that a discrepancy between S and R_H can be negligibly small in a several handers nm thickness in the case of BSTS, where both coefficients are observed with positive sign due to the large contribution of the bulk states. On the other hand, they show negative sign in the film thickness of ca. 14 nm due to the less contribution of the bulk carriers as shown in Fig. 2 and 3. Quantitative discussions between Hall and SdH were able to be made thanks to the high bulk insulating properties of our BSTS films as well as to the accurate thickness dependence of the transport properties.

5. Conclusion

We systematically observed a whole set of electrical transports: longitudinal resistivity (R), transverse Hall (R_H^{2D}) coefficient, Seebeck (S) coefficient, and SdH quantum oscillations, for high quality 3D-TI BSTS as a function of temperature (T) and film thickness (d) in order to clarify the contributions

of both bulk and TSDS carriers. Accurate quantitative discussions were successfully made on the carrier densities of n_{SdH} and $n_{\mathrm{Hall}}^{\mathrm{2D}}$ estimated by both measurements $R_{\mathrm{H}}^{\mathrm{2D}}$ and SdH oscillations. A discrepancy, which has been a debate so far among researchers, was seen between the two types of measurements. D dependences of sheet conductance ($R_{\square}$) and *S* coefficient as a function of *d* clearly show that the semiconducting hole carriers stemming from the bulk states can reasonably be suppressed by reducing *d*, and a topological surface dominant transport was obtained for thin layer films. While $R_{\square}$ and S coefficients were apparently arisen from both the bulk and the surface in the case of thick BSTS films, $R_{\mathrm{H}}^{\mathrm{2D}}$ showed differently that single type carriers arising only from TSDS, even when the contribution from the bulk carriers cannot be negligible. The situation was interpreted in terms of the lager difference in mobility between the surface and the bulk. Cautiously, the carrier density (*n*) of TSDS estimated by $R_{\mathrm{H}}^{\mathrm{2D}}$ provides an overestimate due to the additional influence of the bulk carriers. According to the accurate quantitative comparison of *n* between Hall coefficient ($n_{\mathrm{Hall}}^{\mathrm{2D}}$) and SdH oscillations ($n_{\mathrm{SdH}}$), we showed that a discrepancy gradually becomes small as *d* decreases and importantly $n_{\mathrm{Hall}}^{\mathrm{2D}}$ approaches to a value of almost the twice of n_{SdH}. We propose that Seebeck coefficient can be a very useful and effective probe in order to achieve the intrinsic topological electronic states of 3D-TIs without employing *B* and low *T*.

References

[1] C. L. Kane, and E. J. Mele, *Phys. Rev. Lett.* **95,** 146802 (2005).

[2] M. Z. Hasan, and C. L. Kane, *Rev. Mod. Phys*. **82**, 3045-3067 (2010).

[3] X.-L. Qi, and S.-C. Zhang, *Rev. Md. Phys*. **83**, 1057-1110 (2011).

[4] D. Hsieh, D. Qian, L. Wray, Y. Xia, Y.S. Hor, R.J. Cave, and M.Z. Hasan, Nature 452, 970 (2008).

[5] D. Hsieh, et al., Nature 460, 1101 (2009).

[6] Y. Xia, et al., Nature Phys. 5, 398 (2009).

[7] Y.L. Chen, et al., Science 325, 178 (2009).

[8] J. Zhang, C. Z. Chang, Z. Zhang, J. Wen, X. Feng, K. Li, M. Lui, K. He, L. Wang, X. Chen, Q.-K. Xue, X. Ma, and Y. Wang, *Nature Commun.* **2**, 574 (2011).

[9] Z. Ren, A. A. Taskin, S. Sasaki, K. Segawa, and Y. Ando, Phys. Rev. B 84, 165311 (2011).

[10] A.A. Taskin, Z. Ren, S. Sasaki, K. Segawa, and Y. Ando, *Phys. Rev. Lett.* **107**, 016801 (2011).

[11] T. Arakane, T. Sato, S. Souma, K. Kosaka, K. Nakayama, M. Komatsu, T. Takahashi, Z. Ren, K. Segawa, and Y. Ando, *Nature Commun*. **3**, 636 (2012).

[12] R.J. Cava, H. Ji, M.K. Fuccillo, Q.D. Gibson, and Y.S. Hor, J. Mater. Chem. C **1**, 3176 (2013).

[13] S. K. Kushwaha, et al., Nature Commun. **7,** 11456 (2016).

[14] N. H. Tu, Y. Tanabe, Y. Satake, K. K. Huynh, P. H. Le, S. Y. Matsushita, and K. Tanigaki, *Nano Lett.* 17, 2354 (2017).

[15] Z. Ren, A.A. Taskin, S. Sasaki, K. Segawa, and Y. Ando, Phys. Rev. B 82, 241306(R) (2010).

[16] T. Seebeck, *Annalen der Physik und Chemie*, **6** , 1-20; 133-160; 253-286 (1826).

[17] S.Y. Matsushita, K. K. Huynh, H. Yoshino, N. H. Tu, Y. Tanabe, and K. Tanigaki, Phys. Rev. Mater. 1, 054202 (2017).

[18] J. Zhang, X. Feng, Y. Xu, M. Guo, Z. Zhang, Y. Ou, Y. Feng, K. Li, H. Zhang, L. Wang, X. Chen, Z. Gan, S. -C. Zhang, K. He, X. Ma, Q. -K. Xue, and Y. Wang, *Phys. Rev.* ***B*** **91,** 075431 (2015).

[19] N. H. Tu, Y. Tanabe, Y. Satake, K. K. Huynh, and K. Tanigaki, *Nature commun*. **7,** 13763 (2016).

[20] See Supplemental Material at [] for (1) The morphology of BSTS thin films, (2) Magnetoresistance of BSTS films, (3) Fitting analysis of Hall resistivity with two carrier model.

[21] Solid State Physics, N.W. Ashcroft and N.D. Mermin (Brooks/Cole, Belmont, 1976).

[22] *Thermoelectrics*, G.S. Nolas, J. Sharp, and H.J. Goldsmid (Springer, New York, 2001).

[23] Y. Zhang, et al., Nature Phys. 6, 584 (2010).

[24] A.A. Taskin, S. Sasaki, K. Segawa, and Y. Ando, Phys. Rev. Lett. 109, 066803 (2012).

[25] H. Tang, D. Liang, R.L.J. Qiu, X.P.A. Gao, ACS Nano 5, 7510 (2011).

[26] A.A. Taskin, Y. Ando, Phys. Rev. B 84, 035301 (2011).

[27] T-C. Hsiung, D-Y. Chen, L. Zhao, Y.-H. Lin, C.-Y. Mou, T.-K. Lee, M.-K. Wu, and Y.-Y. Chen, Appl. Phys. Lett. 103, 163111 (2013).

[28] Y. Pan, et al., Solid State Comm. 227, 13 (2016).

[29] B. Xia, P. Ren, A. Sulaev, P. Liu, S.-Q. Shen, and L. Wang, Phys. Rev. B 87, 085442 (2013).

[30] A.H. Castro Neto, F. Guinea, N.M.R. Peres, K.S. Novoselov, and A.K. Geim, Rev. Mod. Phys. 81, 109 (2009).

Acknowledgments

This work was supported in part by a Grant-in-Aid for Scientific Research from the Ministry of Education, Culture, Sports, Science and Technology (MEXT), JSPS KAKENHI Grants No. 17K14329, 18H04471, 17-18H05326, 18H04304, 18H03883, and 18H03858) and thermal management of CREST, JST. This work was sponsored by research grants from Yazaki Memorial Foundation and The Iwatani Naoji Foundation's Research Grant. S.Y.M. thanks Tohoku University Interdepartmental Doctoral Degree Program for Multi-dimensional Materials Science Leaders for financial support. The research is partly carried out by the support of the World Premier International Research Center Initiative (WPI) from MEXT.

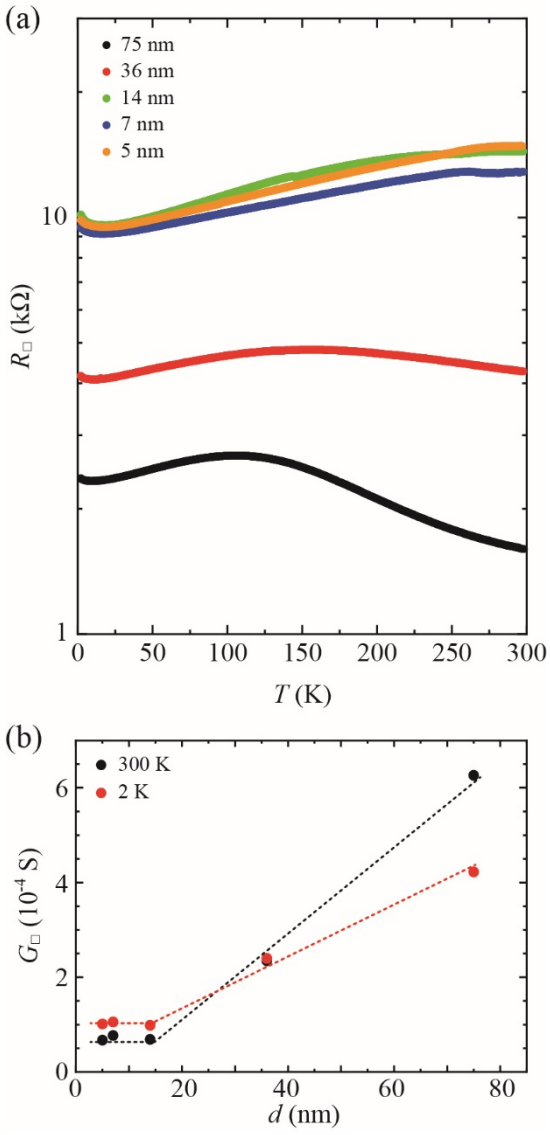

Figure 1. Electrical transport properties of BSTS thin films. (a) Temperature dependence of sheet resistance of BSTS thin films of 75, 36, 14, 7, and 5 nm. (b) Film thickness dependence of total conductance at 300 K (black circles) and 2 K (red circles).

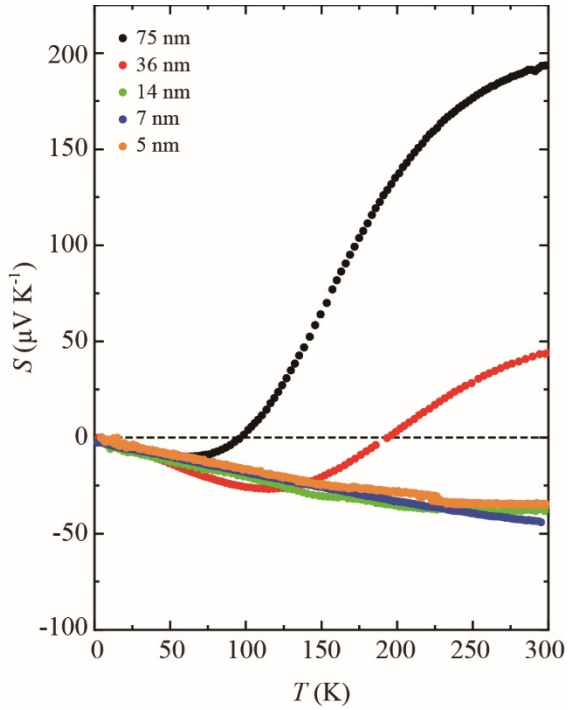

Figure 2. Seebeck coefficient of BSTS thin films. Temperature dependence of Seebeck coefficient (*S*) of BSTS thin films of 75, 36, 14, 7, and 5 nm.

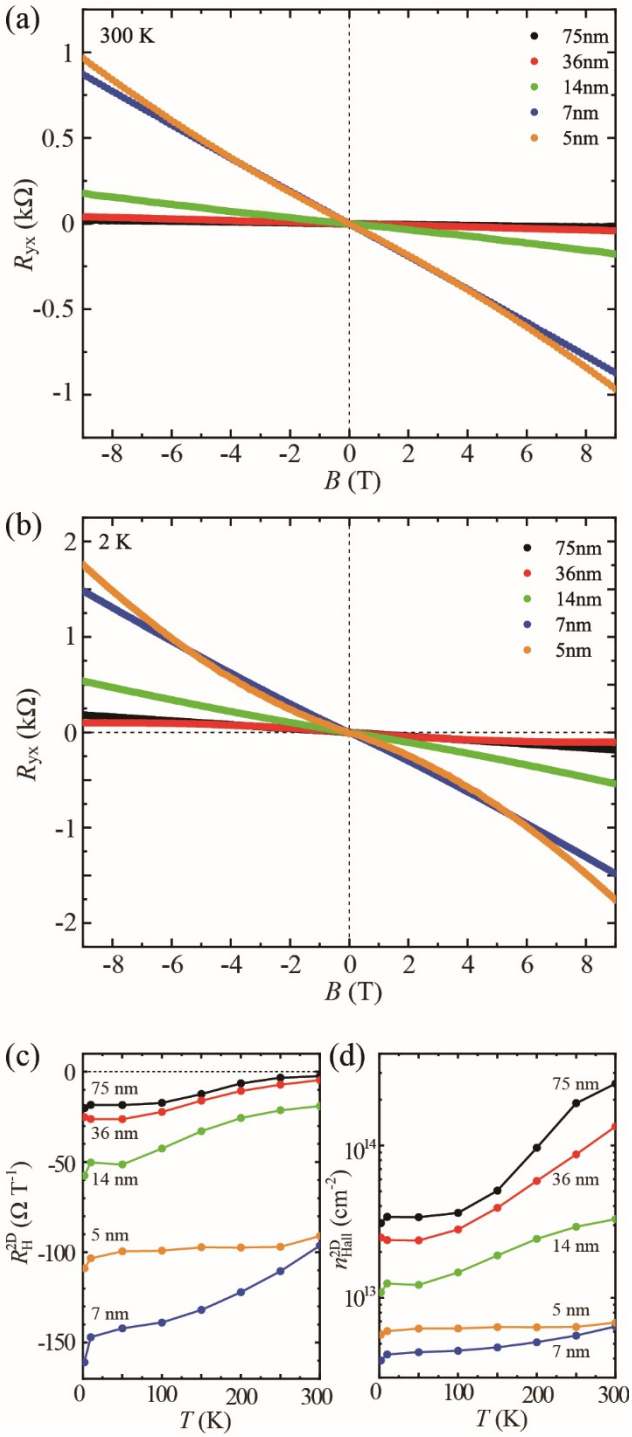

Figure 3. Thickness dependence of Hall resistance of BSTS thin films. Temperature dependence of Hall resistance (R_{yx}) of BSTS thin films of 75, 36, 14, 7, and 5 nm measured at 300 K for (a) and 2 K for (b). (c) two-dimensional Hall coefficient of each film estimated by linear curve fitting within the range of -1 T to 1 T. (d) two-dimensional carrier density of each film.

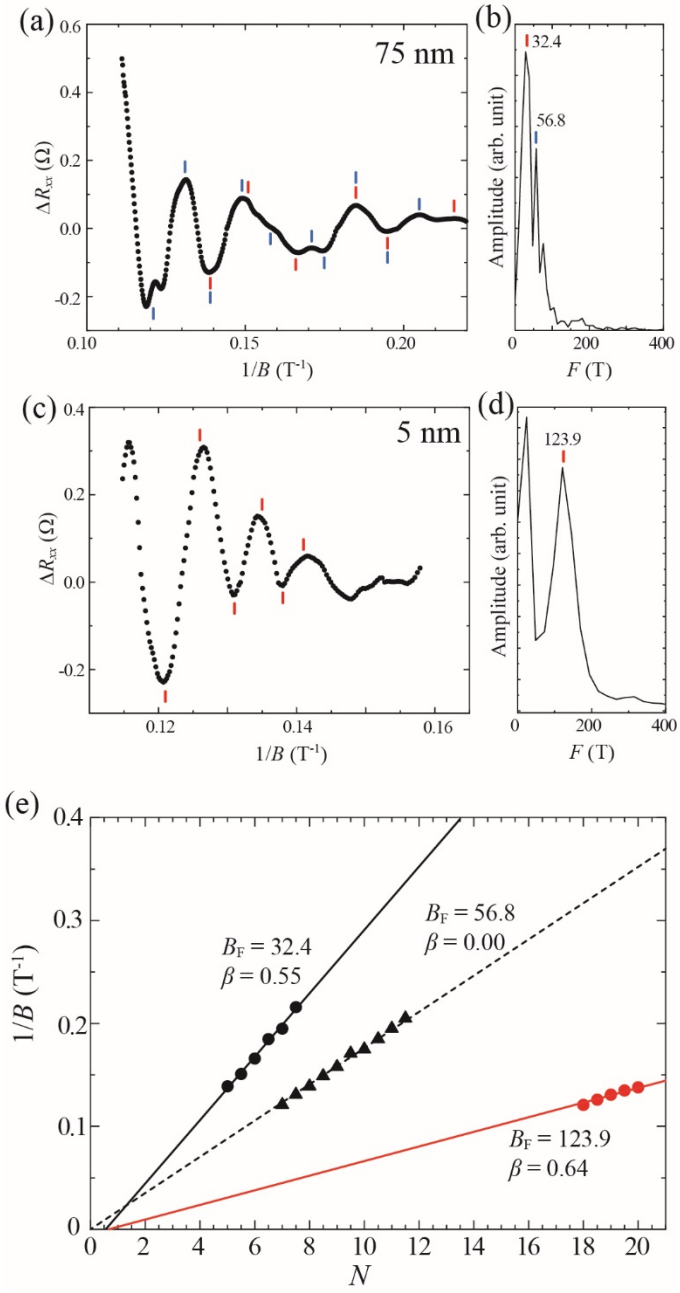

Figure 4. Shubnikov-de-Haase oscillations of BSTS thin films. (a), (c) SdH oscillations of 75 and 5 nm-BSTS films, respectively. Black and red bars indicate the peak and the valley positions. (b), (d) Fast Fourie Transfer (FFT) of the SdH oscillations of 75 and 5 nm BSTS, respectively. (e) Fan-diagram plots of 75 and 5 nm BSTS films, respectively. Black circles and triangles represent the peak and valley positions of 75 nm-BSTS in (a), where circles (triangles) corresponds to the non-trivial TSDS (trivial bulk state) in 3D-TI. Red circles are the peak and valley positions of 5 nm-BSTS in (c) correspond to non-trivial TSDS. The bold and dotted lines are the linear fitting curves for each electronic state.

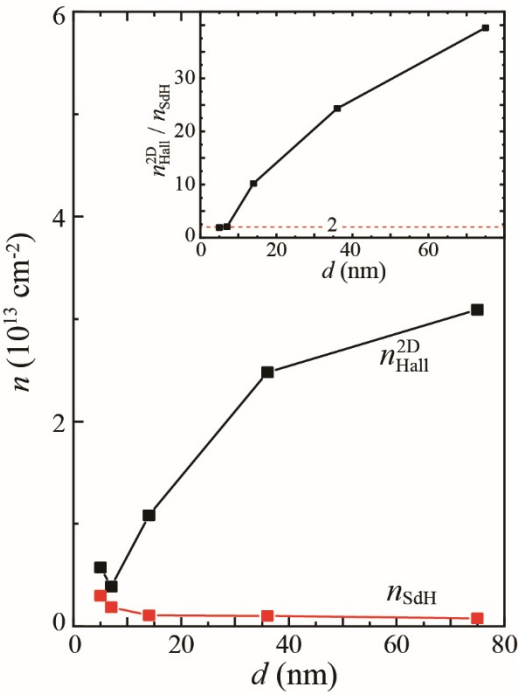

Figure 5. Comparison of carrier density estimated from Hall and SdH oscillation measurements. The thickness dependence of two-dimensional carrier density at 2 K estimated by Hall coefficient (Black) and SdH oscillation (Red). The inset represents the thickness dependence of the ratio $n_{\mathrm{SdH}}/n_{\mathrm{Hall}}^{2\mathrm{D}}$.

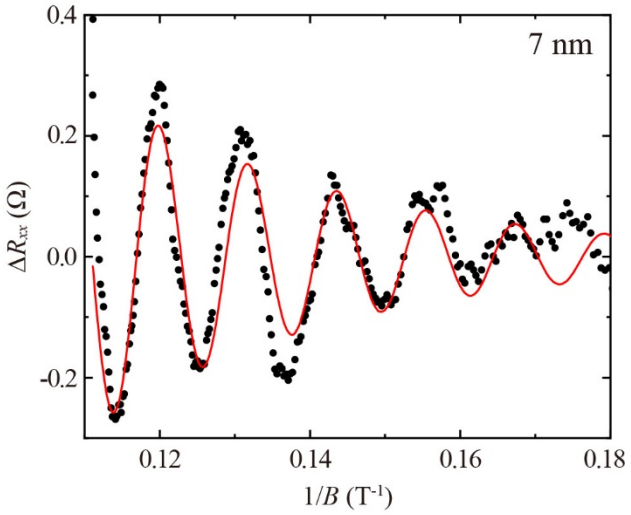

Figure 6. Fitting analysis of Shubnikov-de-Haase oscillations of 7 nm-BSTS thin film. An example of fitting analysis of SdH oscillation of 7 nm-BSTS film. Red curve represents the result of fitting analysis using equation (3) in the text.